Relation between magnetosonic waves and pitch angle anisotropy of warm protons

J. Joseph[1]*, A. N. Jaynes[1], Q. Ma[2,3], D. P. Hartley[1], M. E. Usanova[4] and W. Li[2]

[1]Department of Physics and Astronomy, University of Iowa, Iowa City, IA, United States, [2]Center for Space Physics, Boston University, Boston, MA, United States, [3]Department of Atmospheric and Oceanic Sciences, University of California, Los Angeles, Los Angeles, CA, United States, [4]Laboratory for Atmospheric and Space Physics, University of Colorado Boulder, Boulder, CO, United States

In the past decade, many observations of transversely heated low energy protons were reported in the inner magnetosphere. Interestingly, most of the time heated protons were observed along with magnetosonic waves. Due to the strong correlation, it was often assumed that magnetosonic waves were responsible for the heating of low energy protons. By performing a case study under unusually disturbed geomagnetic conditions, this paper unravels the controversial relationship between the observed pitch angle anisotropy of warm protons and the accompanying magnetosonic waves in the inner magnetosphere. We perform a comparative analysis involving two nearly identical cases of pitch angle anisotropy of warm protons in low L–shell region—one with magnetosonic waves and one without them. It is found that magnetosonic waves are not responsible for primary heating of low-energy protons and may just marginally alter the shape of the distribution of heated protons in the events analyzed. Based on the recent Cluster and POLAR observations, we also show how the recirculated polar wind plasma in the Earth's magnetosphere can cause the concurrent appearance of heated protons and magnetosonic waves.

KEYWORDS

magnetosonic wave, pitch angle anisotropy, wave-particle interaction, polar wind, quasi-linear analysis

Introduction

The evolution of particle pitch angle distributions (PADs) contains vital information on the movements of charged particles and wave-particle interactions. As such, PADs may be used as a diagnostic tool to gain important insights into magnetospheric dynamics. The current study examines certain occurrences of anomalous PADs of the thermal (few eV to tens of eV) and the suprathermal (tens of eV to 100s of eV) protons in the inner magnetosphere. The majority of low-energy ions (tens of eV to hundreds of eV) in the plasmasphere originate from ionospheric outflows (Chappell et al., 1987, 2000, 2008; Huddleston et al., 2005). Typically, ionospheric outflows consist of thermal and suprathermal ions which are guided by the Earth's magnetic field lines and therefore are

expected to have field-aligned PADs (flux peaks around 0°/180°). This expectation was confirmed by Yue et al. (2017) using 4 years of data from Van Allen Probes. Additionally, Yue et al. (2017) showed that, in general, geomagnetic activity does not affect the PADs of protons below several keV. Low-energy proton PADs that peaked around 90° were occasionally reported. Any radial diffusion that transports ions towards Earth can cause an enhancement of perpendicular energy due to conservation of the first and second adiabatic invariants (Schulz & Lanzerotti, 1974). The increase in perpendicular energy leads to a pancake PAD (flux peaks around 90°). Hiss/EMIC waves may cause the transverse heating of very low energy (<1 eV) ions to several eV over long timescales (Artemyev et al., 2017). However, most of the time, pancake PADs of thermal and suprathermal protons are observed in the presence of magnetosonic (MS) waves (Wu et al., 2022). In some recent studies (e.g., Yuan et al., 2018; Ma et al., 2019; Teng et al., 2019; Hill et al., 2020), MS waves were identified as the likely cause of proton heating. But according to the findings of Min et al. (2021), quasilinear diffusion is only effective in heating >1 keV protons and does not influence the thermal/suprathermal proton populations. Moreover, recent statistical studies (Ferradas et al., 2021; Wu et al., 2022) show that despite the possibility for the causal relationship of MS waves and thermal/suprathermal proton pitch angle anisotropy, these features are not strongly associated. But they also noted that the pitch angle anisotropies in the absence of MS waves are typically weaker than when MS waves are present.

Using Van Allen Probes observations of a set of unusually intense magnetospheric events, we reexamine the controversial relationship between MS waves and the pitch angle anisotropy of thermal and suprathermal protons. For the first time, we show that under geomagnetically disturbed conditions, MS waves may not cause the original anisotropy but can change the shape of the anisotropic distribution in accordance with the quasilinear theory.

To find the cause of the pitch angle anisotropy of thermal and suprathermal protons and their correlation with MS waves, a comprehensive examination of all the possible sources of magnetospheric plasma during geomagnetically disturbed conditions is required. Typically, the solar wind is the major source of hot magnetospheric plasma, whilst upward transport from the ionosphere is the source of cold/warm plasma. At high latitudes, streams of ionospheric plasma, known as polar wind, continuously flow out along the open magnetic field lines. Recent studies (Moore et al., 1999; Chappell et al., 2008; Haaland et al., 2012; Chappell et al., 2021) have found that polar wind and polar cusp plasma from ionospheric outflow often gets partially convected back into the magnetosphere. Survey results from polar TIDE observations (Liemohn et al., 2005) and Cluster wake measurements (Engwall et al., 2009b; Andre and Cully, 2012) verify the presence of polar wind particles in the lobes. This normally unaccounted for recirculated plasma can have very significant contributions to magnetospheric dynamics.

Depending on the solar wind parameters, specifically the strength of the southward IMF B_Z, these particles can gain a range of energies that are specific to the plasma sheet, ring current, and warm plasma cloak. Under disturbed geomagnetic conditions, the flow of polar wind substantially increases and Haaland et al. (2012) shows that as much as 90% of it could reenter the magnetosphere. This significant contribution from polar wind under varying strength of southward B_Z enhances the ring current as well as raises the warm plasma population. While the lower energy warm protons travel inwards in their present form preserving the adiabatic invariants, injected ring current protons can cause MS wave generation. To have a complete understanding of the magnetospheric plasma population, it is essential to consider the contribution of the polar wind and polar cusp outflows especially during strong southward B_Z.

In this study, we highlight that simultaneous occurrence of MS waves and pitch angle anisotropy of the thermal and suprathermal proton population could be due to the contribution of polar wind under southward B_Z.

Observations

Here we use wave and particle observations from the Van Allen Probes (Mauk et al., 2013). Wave observations are taken from the Electric and Magnetic Field Instrument Suite and Integrated Science (EMFISIS) (Kletzing et al., 2013). We particularly use the waveform receiver (WFR) of the EMFISIS suite, which provides electric and magnetic field data in the frequency range of ~10 Hz to 12 kHz. Particle data is obtained from the Energetic Particle Composition and Thermal Plasma Suite, in particular the Helium Oxygen Proton Electron (HOPE) instrument, which measures the differential flux and pitch angles of low/medium energy (~1 eV–~50 keV) electrons and ions (Funsten et al., 2013; Spence et al., 2013).

We choose a particularly extended geomagnetically disturbed period with several southward B_Z spikes, which may provide extended observations of pitch angle anisotropy of thermal and suprathermal protons. Figure 1 presents an overview of the unusual magnetospheric conditions under which events of this study occurred on 8 September 2017. The magnetosphere exhibited two successive SYM-H dips of moderate strength (~100–150 nT) within ~12 h interval. Early in the recovery phase of the first storm, a second storm occurred. This event of warm proton anisotropy coincided with the main phase of the second storm. Prior to the event, there were a number of large southward spikes in B_Z. Solar wind speed was ~700 km/s. The AE index also indicates that the second storm hit before the magnetosphere could recover from the first storm.

Van Allen Probe A was traversing away from perigee at an altitude of $\sim 2R_E$ above the Earth's surface during the event. Figure 2 shows the overview of the Van Allen Probe A
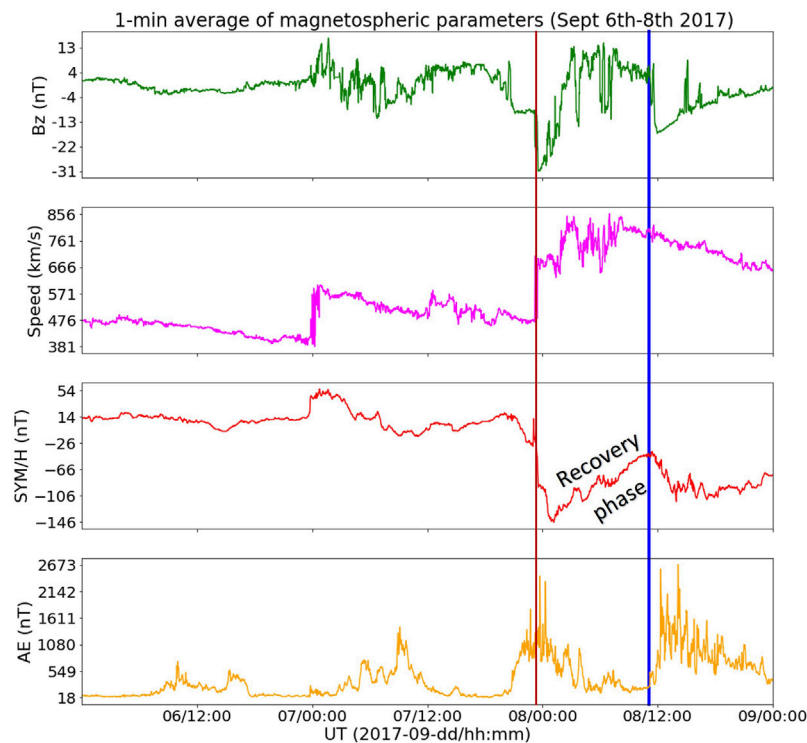
FIGURE 1
Near-earth solar wind parameters and geomagnetic activity indices during the extended disturbed period from 2017-09-06/00 UT to 2017-09-09/00 UT following the large solar X-ray (class X9.3) flare of 6 September 2017. Panels **(A)**, **(B)**, **(C)**, and **(D)** show the magnetic field fluctuations, solar wind speed, SYM-H index, and AE index respectively. The vertical blue line marks the time when the strong pitch angle anisotropy of thermal and suprathermal protons was observed. The vertical red line marks the time of the first storm.

observation demonstrating the remarkable correlation between MS waves and the pitch angle anisotropy of thermal and suprathermal protons. At 10:45–11:10 UT on 8 September 2017, the spacecraft was located over the *L*-shells of 2.5–3.5 near the geomagnetic equator. Figure 2A shows the electron density profile, which is obtained by the EMFISIS instrument using the upper hybrid frequency technique (Kurth et al., 2015). Figures 2B, C show the wave Poynting flux and wave normal angle (WNA). Here we use the Poynting flux that is derived from the sheath-corrected electric field measurements (Hartley et al., 2015, 2016, 2017, 2022). WNAs were estimated by the Singular Value Decomposition (SVD) method (Santolik et al., 2003). To ensure a well-defined WNA, data are only shown (Figure 2C) if the wave planarity exceeds 0.5. This is due to the SVD method relying on the plane wave approximation. The banded waves with frequencies below the lower hybrid frequency, very oblique WNA (~90˚) and linear polarization (Figure 2D), are identified as MS waves. Figure 2E shows the overall proton flux observed by HOPE. Pitch angle distributions of protons at energies of ~21 eV and ~450 eV are shown in Figure 2F and 2G. The vertical dashed lines on Figure 2 are provided to highlight the apparent correlation between the

pitch angle anisotropy of thermal and suprathermal protons and the intensity of MS waves. In order to quantify the capability of MS waves in heating the low-energy protons, in the next section we carry out a detailed analysis of the observed wave-particle interactions during the event.

We also record a second case of pitch angle anisotropy of thermal and suprathermal proton under similar condition at 09:00 to 09:15 UT, a summary of which is shown in Figure 5. There were no MS waves observed during that interval.

Analysis

To determine the dependency of pitch angle anisotropy of thermal and suprathermal protons on MS waves, we conduct a comparative study. We choose two adjacent time intervals at 10:45-10:57 UT and at 10:57-11:05 UT with anisotropic pitch angle distributions of thermal and suprathermal protons (Figure 2F and 2G). The later interval had substantially larger MS wave intensities compared to the earlier one (Figure 2B). Poynting flux of the MS waves and spin-averaged flux density of thermal and suprathermal protons
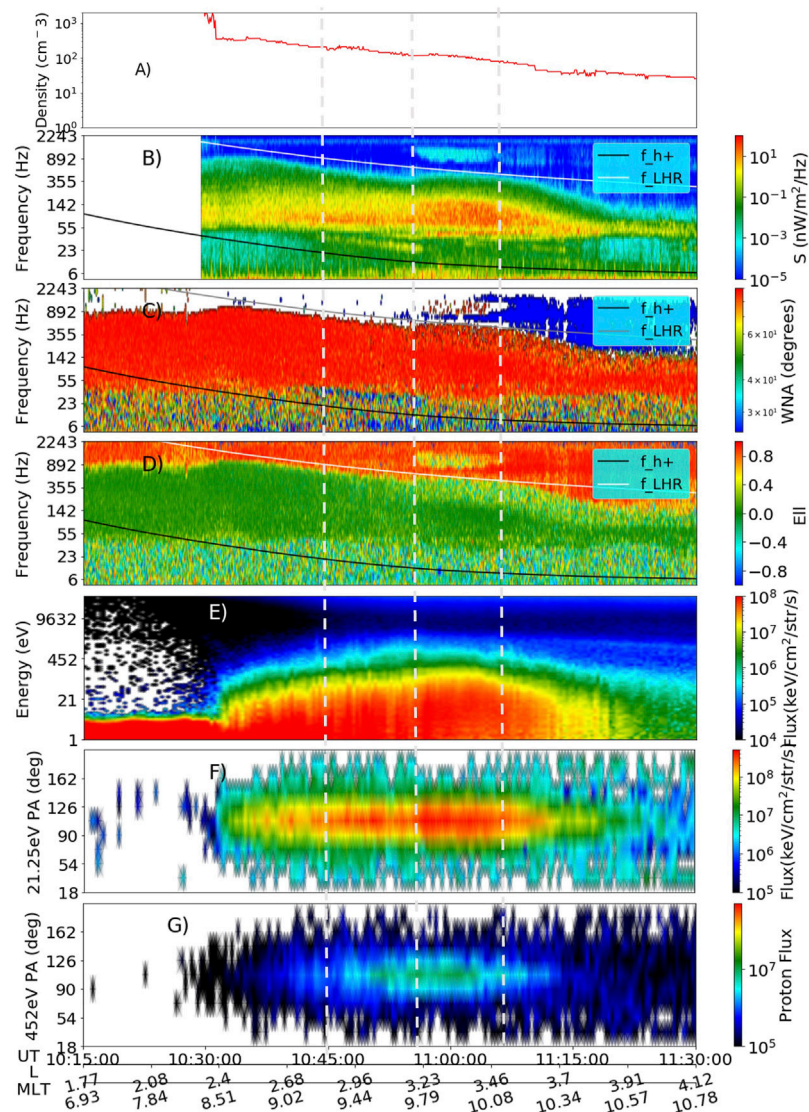
FIGURE 2
Correlation between thermal and suprathermal proton pancake pitch angle distributions (PADs) and the magnetosonic (MS) waves observed by Van Allen Probe A on 8 September 2017. Panel **(A)** shows the electron density profile. Panel **(B)** shows the Poynting flux density, panel **(C)** shows the wave normal angle, and panel **(D)** shows the ellipticity of the magnetic field polarization, in the frequency range from 5 to 2000 Hz. In panels **(B)**, **(C)**, and **(D)**, the white and the black traces represent lower hybrid resonance frequency and proton cyclotron frequency, respectively. Electron density data and sheath corrected Poynting vector data (shown in panels A and B) are not available between 10:15 and 10:30 UT. Energy spectrogram of spin-averaged proton flux is shown in panel **(E)**. Pitch angle distributions of proton fluxes at energies of ~21 eV and ~450 eV are shown in panels **(F)** and **(G)** respectively. The vertical white dashed lines mark the time intervals with different MS wave intensity, subsections of which are used for quasilinear analysis.

are shown in Panels A–B of Figure 3, respectively. Panels C1 and C2 of Figure 3 show the PADs of thermal and suprathermal protons at three different energies (21 eV, 98 eV, and 450 eV) for the two time intervals. Even though the general appearance of the distribution in both Figure 3 C1 and Figure 3C2 follows a pancake shape, there are subtle differences–in Figure 3C1, the lower energy (~21 eV, red trace) protons have a cap-like (also called head-and-

shoulder) distribution and in Figure 3C2, the higher energy (~450 eV, blue trace) protons have a cap-like distribution.

We perform a quasi-linear analysis of the MS waves in the two adjacent time intervals, at 10:52-10:57 UT and at 10:58-11:03 UT. Note that to limit the change in satellite L-shell, we use a slightly shorter time interval compared to the total duration of the observation. Figure 4 shows the result of the quasi-linear analysis. Top row (black traces) shows the continuous power
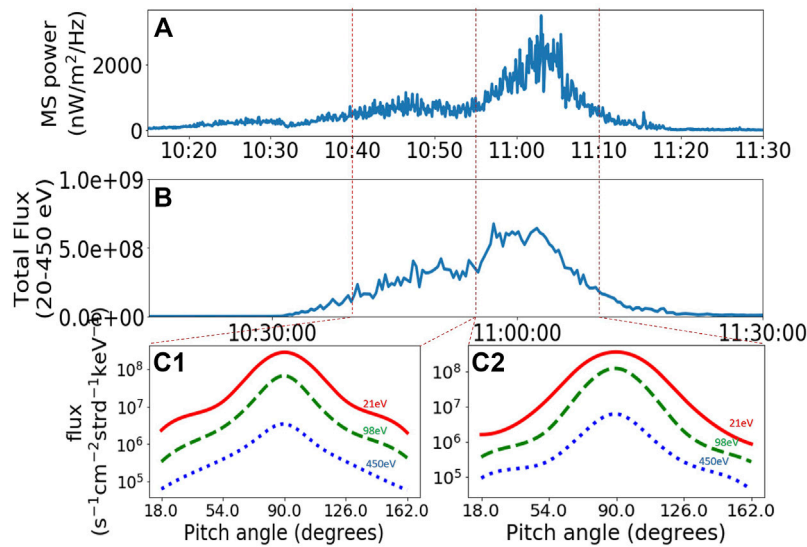
FIGURE 3
Comparison of pitch angle distribution of thermal/suprathermal protons in two adjacent time intervals. Panel **(A)** shows the Poynting flux density of MS waves. Panel **(B)** shows the flux density of protons in the energy range of 21−450 eV. Panel **(C1)**, **(C2)** shows the pitch angle distributions of protons at energies 21 eV (red), 98 eV (green), and 450 eV (blue).

spectrum of the magnetic field intensity as recorded by the EMFISIS WFR. However, this power spectrum could have hidden harmonic structures with high intensity near frequencies of $N f_{cp}$, where N is the harmonic number and f_{cp} is the proton cyclotron frequency, which might have been overlooked due to the limited frequency resolution of WFR in survey mode. But the wave intensity close to each frequency $N f_{cp}$ is important for the resonant interaction with lower-energy protons. In order to estimate the maximum possible heating effects on low-energy protons, we create a harmonic wave frequency spectrum of the MS waves (Figure 4A, red traces). For the waves observed at frequencies from $(N - 0.5)^* f_{cp}$ to $(N + 0.5)^* f_{cp}$ by WFR, we produce a Gaussian wave frequency spectrum in the form of $e^{-\frac{(f-N^*f_{cp})^2}{(0.1^*f_{cp})^2}}$, conserving the total wave power around each harmonic. As shown in Figure 4A, the assumed wave power spectrum with harmonic structure has large intensity at each harmonic of N*f_{cp} with a narrow frequency width. We use the assumed wave power spectrum to quantify the interaction between protons and MS waves with harmonic frequency structures as previously observed (e.g., Balikhin et al., 2015). Although the assumed wave frequency spectrum (red traces in Figure 4A) may deviate from the realistic spectrum as the MS waves propagate (Ma et al., 2014a,b), it provides an estimate of the maximum proton heating efficiency at low energies.

We use the Full Diffusion Code to calculate the bounce-averaged diffusion coefficients of protons due to MS waves (Ma et al., 2019). MS waves are assumed to have a latitude coverage from the equator to 5°. The wave normal angle (θ) is assumed to

follow a Gaussian distribution in X = tan(θ), which is proportional to $e^{-(X-X_m)^2/(X_w)^2}$, for $X_{LC}\langle X \langle X_{UC}$. The central wave normal angle X_m = tan (89.3°), the width X_w = tan (88.8°), the upper cutoff X_{UC} = tan (89.9°), and the lower cutoff X_{LC} = tan (87°). We include the harmonic resonance numbers from -10 to 50. The wave frequency spectrum, wave amplitude, total electron density and background magnetic field are from observations and are presented in Figure 4A.

The continuous spectrum (black traces in Figure 4A) is used to calculate the pitch angle diffusion coefficients $D_{\alpha\alpha}$ and momentum diffusion coefficients D_{EE}, as shown in Figure 4B. The bottom row (Figure 4C) shows the calculated $D_{\alpha\alpha}$ and D_{EE} if the waves contained the harmonic structures (red traces in Figure 4A). As seen from the analysis, the main wave-particle interaction regions are concentrated in the energy range of tens of keV. This is expected as the energy source of MS waves are related to ring current protons (Meredith et al., 2008; Chen et al., 2010; Jordanova et al., 2012; Ma et al., 2014a). Also, for these nearly perpendicularly propagating waves, pitch angle diffusion coefficients $D_{\alpha\alpha}$ are smaller than the momentum diffusion coefficients D_{EE}. From the middle panels (Figure 4B), it is evident that the continuous power spectrum of MS waves has negligible effect on protons below the energy of 1 keV, which is in line with the findings of Min et al. (2021). For the discrete spectrum, the interaction at lower energy increases as the waves' resonant energy drops down to thermal energy range every time the wave frequency (f) is close to a harmonic $f = N f_{cp}$. Comparison of Figures 4C2 and 4C4 shows that MS waves have larger effects on low energy protons (tens of eV) during
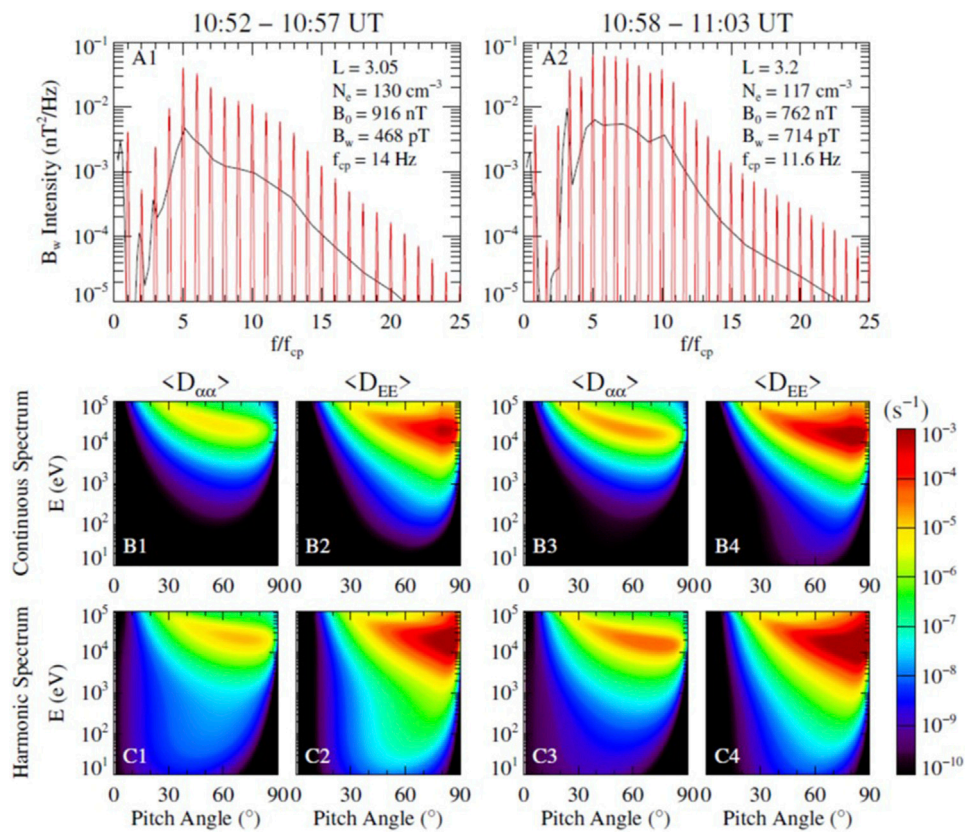
FIGURE 4
Quasi-linear analysis of MS waves interacting with protons during two adjacent time intervals. Black traces in **(A1,A2)** are the observed magnetic power spectral densities (PSDs) of MS waves. Corresponding assumed harmonic PSDs (red) are overplotted. Panels **(B1,B2)** show the pitch angle and momentum diffusion coefficients derived from the continuous PSD shown in A1. Corresponding diffusion coefficients derived from the discrete PSD are shown in panels **(C1,C2)**. Same format is followed for **(B3,B4)**, **(C3,C4)** for the PSDs in A2.

the interval prior to 10:57 UT, but the higher energy protons (hundreds of eV) are more affected during the later interval. Interestingly, we have also seen changes in the shapes of the PADs in the two intervals from the observational data (Figure 3C1 and 3C2). Prior to 10:57 UT, lower energy protons had a cap-like distribution and after 10:57 UT higher energy protons had a cap-like distribution. We speculate that the MS waves may have some contribution in generating the cap distributions. The diffusion coefficients during the second interval are more concentrated towards high pitch angles (Figures B4 and C4) than those during the first interval (Figures B2 and C2). But, the diffusion coefficients are in general small for the energies below 100 eV.

It is to be noted that the diffusion coefficients and proton heating efficiency due to MS waves depend on the wave normal angle and latitude distribution. Recent observations have shown MS waves at higher latitudes than 10° (Boardsen et al., 2016; Wu et al., 2021), which may have smaller wave normal angles. We performed tests of the diffusion coefficient calculations using

different wave normal angle distributions (not shown). Although the energy diffusion coefficients are higher when the central wave normal angle is a few degrees lower than 89.3°, the timescale of proton heating is still longer than 1 day at the energies below several hundred eV. The magnetosonic waves generated at high latitudes could cause additional heating of protons at low pitch angles, but may not directly affect the protons with large pitch angles which mirror between low magnetic latitudes.

Discussion

Our analysis shows that MS waves mainly affect protons at pitch angles ~30°–60° instead of ~90° in the energy range of 10–450 eV. Moreover, the low diffusion coefficients, which correspond to timescales of at least several days for the discrete wave frequency spectrum, cannot explain the simultaneous appearance of MS waves and anisotropic PADs of low-energy protons. So, it is unlikely that MS waves can cause the formation of the pancake/cap distribution
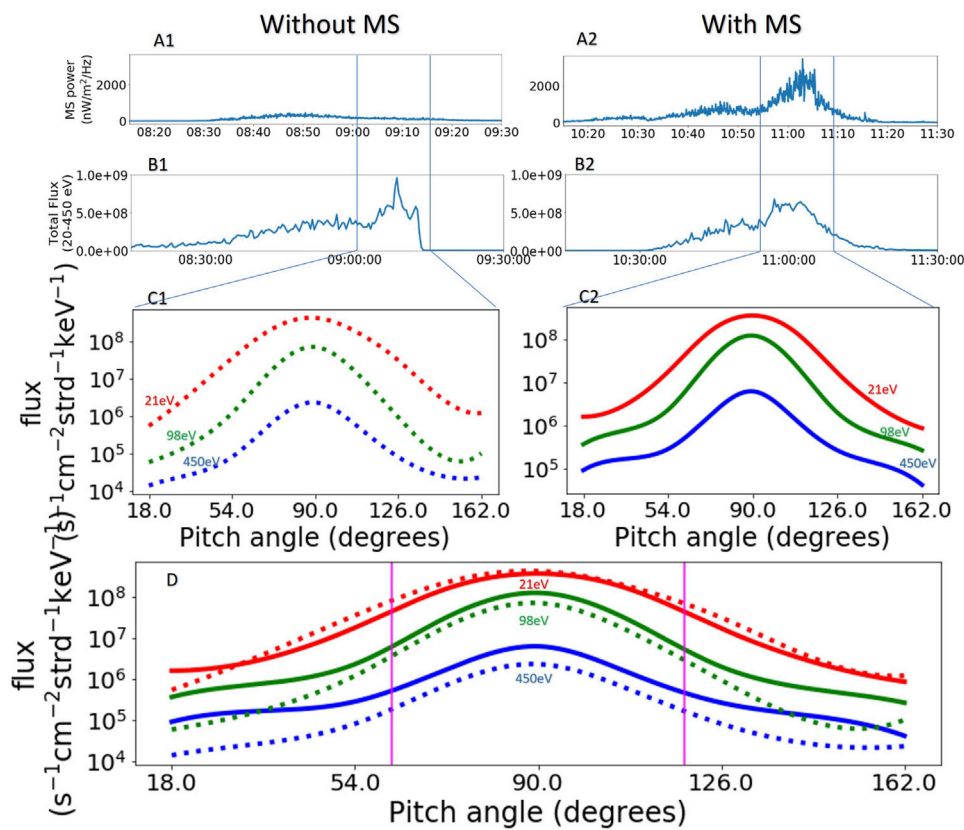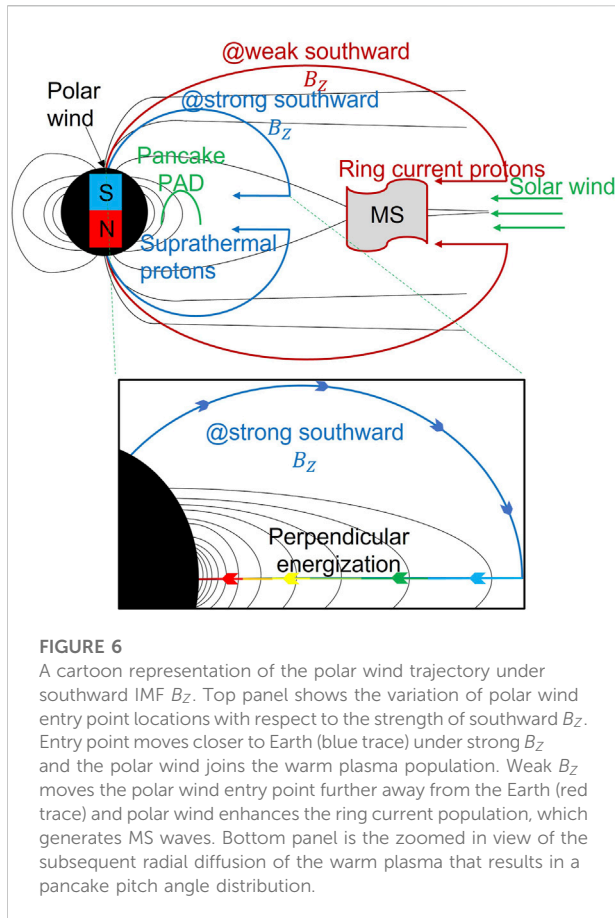
FIGURE 5
Comparison of pitch angle distribution of thermal/suprathermal protons in the presence and absence of MS waves. Panel **(A1,A2)** shows the Poynting flux of MS waves. Panel **(B1,B2)** shows the flux density of protons in the energy range of 20−450 eV. Panel **(C1,C2)** shows the pitch angle distributions of protons at energies of 21 eV (red), 98 eV (green), and 450 eV (blue). Distribution plots of panel C1 (dotted) and C2 (solid) are overplotted in panel **(D)** for comparison. Magenta vertical lines on panel D marks the regions of pitch angles around 90° beyond which the shapes of the distribution (solid and dotted lines) differ substantially for higher energies (green and blue traces).

from the ambient field-aligned distribution of protons at energies below 100 eV. A very similar conclusion was drawn in a recent statistical study by Wu et al. (2022). We also excluded the effect of EMIC waves since no significant EMIC waves were detected during this event. This leads us to doubt the validity of the assumption that local wave-particle interaction is the main cause of the observed proton heating. However, the quasi-linear analysis shows that MS waves can marginally affect the pitch angle anisotropy of protons. For conclusive observational evidence, we need another event of pitch angle anisotropy of similar severity without MS waves. On the day of the event, 8 September 2017, we came across another event, which matched this criterion. Van Allen Probe A crossed the low L-shell region (2.1 < L < 2.5) for the inbound pass and (3.1 < L < 3.5) for the outbound pass within 2 hours and encountered a pitch angle anisotropy of similar strength at both the regions. Strong MS waves were detected during the outbound pass (10:55–11:10 UT) as opposed to negligible MS waves during the inbound pass (09: 00–09:15 UT) as shown in Figure 5A. We have already examined the effect of the MS waves on thermal and

suprathermal protons during the outbound pass (Figures 4B4, 4C4). During the inbound pass at the earlier time, thermal/ suprathermal protons were not affected by MS waves. We see a clear increase in thermal and suprathermal proton flux density at 09: 00–09:15 UT and at 10:55–11:10 UT during the inbound and the outbound passes (Figure 5B). We plot the cumulative fluxes of protons with energies 21 eV (red), 98 eV (green) and 450 eV (blue) at various pitch angles in Figure 5C, for the two time intervals. As evident from Panels B and C of Figure 5, both the total flux density and the pitch angle anisotropy of the 21 eV, 98 eV, and 450 eV protons were approximately identical during the two intervals. To compare and contrast the distribution shape, two time slices shown in Figure 5C are overlapped and plotted in Figure 5D. We see that the distributions coincide for the low energy protons (red traces). At higher energies (green and blue traces), the two distributions match around the center (90° ± 30°) but deviates substantially away from each other at the fringes. Thermal and suprathermal protons have higher fluxes at low pitch angles in presence of MS waves. This is the result we expected from the quasilinear analysis (Figures 4B,C). Our

FIGURE 6
A cartoon representation of the polar wind trajectory under southward IMF B_Z. Top panel shows the variation of polar wind entry point locations with respect to the strength of southward B_Z. Entry point moves closer to Earth (blue trace) under strong B_Z and the polar wind joins the warm plasma population. Weak B_Z moves the polar wind entry point further away from the Earth (red trace) and polar wind enhances the ring current population, which generates MS waves. Bottom panel is the zoomed in view of the subsequent radial diffusion of the warm plasma that results in a pancake pitch angle distribution.

analysis result (Figure 4B and 4C4) shows that MS waves have negligible effects on very low energy (~10–20 eV) protons. Though, higher energy protons (~100–500 eV) with pitch angles away from 90° can be energized by MS waves. This serendipitous observation proves that MS waves can alter the shape of the PAD of thermal and suprathermal protons from pancake to cap but another non-local source is required to supply the initial anisotropic proton fluxes.

One potential means of producing a pancake PAD at low energies is by additional proton injections and their subsequent radial diffusion. To conserve the first and second adiabatic invariants, proton pitch angles become larger as they travel towards regions of higher magnetic field strength, in otherwards to lower L-shells. We investigate the possible mechanism of particle injections under the geomagnetic conditions preceding the event. Recent theoretical and observational studies have shown that the cold (a few eV) polar wind that flows continuously upward from the ionosphere often reenters the magnetosphere. The polar wind convection process intensifies under geomagnetically disturbed conditions. The injected protons from the polar wind can get accelerated and eventually acquire energies typical of the ring current and/or the warm plasma cloak (Chappell et al., 2021). Figure 6 (top panel) is a cartoon representation of the polar wind trajectories under southward IMF B_Z. Haaland et al. (2012), using data from the Cluster mission, mapped the movement of the outflowing polar wind stream. They show how the trajectory of the polar wind stream changes with respect to the direction of the IMF B_Z. According to their estimate, 90% of the polar wind would exhaust out of the back of the tail during northward B_Z. But, under southward B_Z, most of the polar wind is directed into the Earth's plasma sheet region. Importantly, as the strength of the southward B_Z increases, the reentry point of the polar wind moves closer to the Earth. POLAR satellite observations reported by Moore et al. 1999) also had very similar findings. Outflow that enters closer to the Earth (shown as the blue trace in Figure 6) gains less energy and makes the warm plasma cloak (Chappell et al., 2008). Whereas particles that enter further away from the Earth (shown as the red trace in Figure 6) can attain ring current energies (10s of keV) due to the effect of the cross-tail potential, reconnection and betatron acceleration (Huddleston et al., 2005). These injected protons, both ring current and warm plasma, would have pancake PADs due to conservation of the first and the second adiabatic invariants as they diffuse Earthwards. So, the wide range of B_Z (-30 to +10 nT) prior to the event possibly caused both thermal and suprathermal proton injections as well as ring current enhancements. MS waves are generated from the ring current ions. Thus, it is not surprising that MS waves and anisotropic PADs of thermal and suprathermal protons are often observed simultaneously.

Conclusion

Thermal/suprathermal proton heating by MS wave is a controversial issue. The concurrent occurrences of pancake PADs and MS waves seemingly suggests that MS waves contribute to the formation of pancake PADs in low energy protons. On the one hand, past studies have shown that under special circumstances, e.g., in the density cavity of the plasmasphere, MS waves can heat cold H^+ and He^+ ions (Yuan et al., 2018) or MS waves with substantial $k\parallel$ component could heat cold protons (Sun et al., 2017). On the other hand, Min et al. (2021) found that the quasilinear diffusion process is ineffective for heating cold protons to thermal/suprathermal energies. According to the large statistical study involving 46,253 events over 5 years, Wu et al. (2022) found no evidence that, in general, MS waves are able to directly cause the formation of the pancake distribution of warm protons. Our case study supports this conclusion. We show that the pitch angle anisotropy observed in thermal/suprathermal protons need not always be caused by local wave-particle interactions. Powerful injections of polar wind plasma into the magnetosphere under varying southward IMF B_Z generates both warm protons as well as ring current proton populations. As the warm protons travel Earthward, to preserve the first and second adiabatic invariants, a pancake PAD emerges. At the same time, ring current protons cause MS wave, which travel radially and azimuthally. Even though the MS waves do not cause the initial pitch angle anisotropy in thermal/suprathermal protons, we show that the wave-particle interaction may change the shape of the

PAD from pancake to cap, which agrees with the theory. The main findings of this paper are summarized below:

- Magnetosonic (MS) waves are inefficient in heating protons with energies below a few hundred eV despite their frequently synchronized occurrences.
- Polar wind under southward B_Z can cause the simultaneous appearance of MS waves and pancake pitch angle distributions of warm protons.
- MS waves can only slightly affect the energies of warm protons at mid-range pitch angles, which may alter the shape of a preexisting pancake distribution to a cap distribution.

The observational evidence of polar wind is not provided in this paper. However, from previous studies (Moore et al., 1999; Chappell et al., 2008; Haaland et al., 2012; Chappell et al., 2021) polar wind is expected to be present during all south ward B_Z conditions. A detailed statistical study is needed in the future to evaluate the role of the polar wind in causing the concurrent appearance of perpendicularly heated warm plasma with MS waves. Simulations and/or theoretical estimates are also needed to quantify this effect.

At this point, all descriptions of the polar wind affecting the PADs of thermal/suprathermal protons and generating MS waves are speculation. No supporting observations exists as of now.

Data availability statement

Van Allen Probes HOPE data is available from the ECT Science Operations and Data Center, https://rbsp-ect. newmexicoconsortium.org/data_pub/, EMFISIS data from http://emfisis.physics.uiowa.edu. Solar wind data is available from https://omniweb.gsfc.nasa.gov/form/omni_min.html.

Author contributions

Funding

Conflict of interest

The authors declare that the research was conducted in the absence of any commercial or financial relationships that could be construed as a potential conflict of interest.

Publisher's note

References

André, M., and Cully, C. M. (2012). Low-energy ions: A previously hidden solar system particle population. *Geophys. Res. Lett.* 39, L03101. doi:10.1029/2011gl050242

Artemyev, A. V., Mourenas, D., Agapitov, O. V., and Blum, L. (2017). Transverse eV ion heating by random electric field fluctuations in the plasmasphere. *Phys. Plasmas* 24 (2), 022903. doi:10.1063/1.4976713

Balikhin, M., Shprits, Y., Walker, S., Chen, L., Cornilleau-Wehrlin, N., Dandouras, I., et al. (2015). Observations of discrete harmonics emerging from equatorial noise. *Nat. Commun.* 6, 7703. doi:10.1038/ncomms8703

Boardsen, S. A., Hospodarsky, G. B., Kletzing, C. A., Engebretson, M. J., Pfaff, R. F., Wygant, J. R., et al. (2016). Survey of the frequency dependent latitudinal distribution of the fast magnetosonic wave mode from Van Allen Probes Electric and Magnetic Field Instrument and Integrated Science waveform receiver plasma wave analysis. *J. Geophys. Res. Space Phys.* 121, 2902–2921. doi:10.1002/2015JA021844

Chappell, C. R., Giles, B. L., Moore, T. E., Delcourt, D. C., Craven, P. D., and Chandler, M. O. (2000). The adequacy of the ionospheric source in supplying magnetospheric plasma. *J. Atmos. Sol. Terr. Phys.* 62, 421–436. doi:10.1016/s1364-6826(00)00021-3

Chappell, C. R., Glocer, A., Giles, B. L., Moore, T. E., Huddleston, M. M., and Gallagher, D. L. (2021). The key role of cold ionospheric ions as a source of hot magnetospheric plasma and as a driver of the dynamics of substorms and storms. *Front. Astron. Space Sci.* 8, 746283. doi:10.3389/fspas.2021.746283

Chappell, C. R., Huddleston, M. M., Moore, T. E., Gilse, B. L., and Delcourt, D. C. (2008). Observations of theWarm plasma cloak and an explanation of its formation in the magnetosphere. *J. Geophys. Res.* 113, A09206. doi:10.1029/2007ja012945

Chappell, C. R., Moore, T. E., and Waite, J. H., Jr. (1987). The ionosphere as a fully adequate source of plasma for the Earth's magnetosphere. *J. Geophys. Res.* 92, 5896. doi:10.1029/ja092ia06p05896

Chen, L., Thorne, R. M., Jordanova, V. K., and Horne, R. B. (2010). Global simulation of magnetosonic wave instability in the storm time magnetosphere. *J. Geophys. Res.* 115, A11222. doi:10.1029/2010JA015707

Engwall, E., Eriksson, A. I., Cully, C. M., Andre, M., Torbert, R., and Vaith, H. (2009b). Earth's ionospheric outflow dominated by hidden cold plasma. *Nat. Geosci.* 2 (24), 24–27. doi:10.1038/ngeo387

Ferradas, C. P., Boardsen, S. A., Fok, M. C., Buzulukova, N., Reeves, G. D., and Larsen, B. A. (2021). Observations of density cavities and associated warm ion flux enhancements in the inner magnetosphere. *JGR. Space Phys.* 126 (3), e28326. doi:10.1029/2020JA028326

Funsten, H., Skoug, R., Guthrie, A., MacDonald, E., Baldonado, J., Harper, R., et al. (2013). Helium, Oxygen, Proton, and Electron (HOPE) mass spectrometer for the radiation belt storm probes mission. *Space Sci. Rev.* 179 (1-4), 423–484. doi:10.1007/s11214-013-9968-7

Haaland, S., Eriksson, A., Engwall, E., Lybekk, B., Nilsson, H., Pedersen, A., et al. (2012). Estimating the capture and loss of cold plasma from ionospheric outflow. *J. Geophys. Res.* 117, A07311. doi:10.1029/2012ja017679

Hartley, D. P., Chen, L., Christopher, I. W., Kletzing, C. A., Santolik, O., Li, W., et al. (2022). The angular distribution of lower band chorus waves near plasmaspheric plumes. *Geophys. Res. Lett.* 49, e2022GL098710. doi:10.1029/2022gl098710

Hartley, D. P., Chen, Y., Kletzing, C. A., Denton, M. H., and Kurth, W. S. (2015). Applying the cold plasma dispersion relation to whistler mode chorus waves: EMFISIS wave measurements from the van allen probes. *J. Geophys. Res. Space Phys.* 120, 1144–1152. doi:10.1002/2014JA020808

Hartley, D. P., Kletzing, C. A., Kurth, W. S., Bounds, S. R., Averkamp, T. F., Hospodarsky, G. B., et al. (2016). Using the cold plasma dispersion relation and whistler mode waves to quantify the antenna sheath impedance of the Van Allen Probes EFW instrument. *J. Geophys. Res. Space Phys.* 121, 4590–4606. doi:10.1002/2016JA022501

Hartley, D. P., Kletzing, C. A., Kurth, W. S., Hospodarsky, G. B., Bounds, S. R., Averkamp, T. F., et al. (2017). An improved sheath impedance model for the Van Allen Probes EFW instrument: Effects of the spin axis antenna. *J. Geophys. Res. Space Phys.* 122, 4420–4429. doi:10.1002/2016JA023597

Hill, S., Buzulukova, N., Boardsen, S., and Fok, M. C. (2020). Local heating of oxygen ions in the presence of magnetosonic waves: Possible source for the warm plasma cloak? *JGR. Space Phys.* 125 (8), e27210. doi:10.1029/2019JA027210

Huddleston, M. M., Chappell, C. R., Delcourt, D. C., Moore, T. E., Giles, B. L., and Chandler, M. O. (2005). An examination of the process and magnitude of ionospheric plasma supply to the magnetosphere. *J. Geophys. Res.* 110 (12), A12202. doi:10.1029/2004ja010401

Jordanova, V. K., Welling, D. T., Zaharia, S. G., Chen, L., and Thorne, R. M. (2012). Modeling ring current ion and electron dynamics and plasma instabilities during a high speed stream driven storm. *J. Geophys. Res.* 117, A00L08. doi:10.1029/2011JA017433

Kletzing, C., Kurth, W., Acuna, M., MacDowall, R., Torbert, R., Averkamp, T., et al. (2013). "The electric and magnetic field instrument suite and integrated science (EMFISIS) on RBSP," in *The van allen Probes mission* (New York, USA: Springer), 127–181. doi:10.1007/s11214-013-9993-6

Kurth, W. S., De Pascuale, S., Faden, J. B., Kletzing, C. A., Hospodarsky, G. B., Thaller, S., et al. (2015). Electron densities inferred from plasma wave spectra obtained by the Waves instrument on Van Allen Probes. *JGR. Space Phys.* 120, 904–914. doi:10.1002/2014JA020857

Liemohn, M. W., Moore, T. E., Craven, P. D., Maddox, W., Nagy, A. F., and Kozyra, J. U. (2005). Occurrence statistics of cold, streaming ions in the near-earth magnetotail: Survey of polar-TIDE observations. *J. Geophys. Res.* 110, A07211. doi:10.1029/2004ja010801

Ma, Q., Li, W., Chen, L., Thorne, R. M., and Angelopoulos, V. (2014a). Magnetosonic wave excitation by ion ring distributions in the Earth's inner magnetosphere. *JGR. Space Phys.* 119, 844–852. doi:10.1002/2013JA019591

Ma, Q., Li, W., Chen, L., Thorne, R. M., Kletzing, C. A., Kurth, W. S., et al. (2014b). The trapping of equatorial magnetosonic waves in the Earth's outer plasmasphere. *Geophys. Res. Lett.* 41, 6307–6313. doi:10.1002/2014GL061414

Ma, Q., Li, W., Yue, C., Thorne, R. M., Bortnik, J., Kletzing, C. A., et al. (2019). Ion heating by electromagnetic ion cyclotron waves and magnetosonic waves in the Earth's inner magnetosphere. *Geophys. Res. Lett.* 46 (12), 6258–6267. doi:10.1029/2019GL083513

Mauk, B., Fox, N. J., Kanekal, S., Kessel, R., Sibeck, D., and Ukhorskiy, A. A. (2013). Science objectives and rationale for the radiation belt storm probes mission. *Space Sci. Rev.* 179 (1–4), 3–27. doi:10.1007/s11214-012-9908-y

Meredith, N., Horne, R. B., and Anderson, R. R. (2008). Survey of magnetosonic waves and proton ring distributions in the Earth's inner magnetosphere. *J. Geophys. Res.* 113, A06213. doi:10.1029/2007JA012975

Min, K., Kim, J., Ma, Q., Jun, C., and Liu, K. (2021). Unusual high frequency EMIC waves: Detailed analysis of EMIC wave excitation and energy coupling between EMIC and magnetosonic waves. *Adv. Space Res.* 69 (2022), 35–47. doi:10.1016/j.asr.2021.07.039

Moore, T., Chandler, M. O., Chappell, C. R., Comfort, R. H., Craven, P. D., Delcourt, D. C., et al. (1999). "Polar/TIDE results on polar outflows,". Editors J. L. Burch, R. L. Carovillano, and S. K. Antiochos, (Washington, D. C: AGU), 109, 87.*Sun-Earth Plasma Connect. Geophys. Monogr. Ser.*

Santolik, O., Parrot, M., and Lefeuvre, F. (2003). Singular value decomposition methods for wave propagation analysis. *Radio Sci.* 38 (1), 1010. doi:10.1029/2000RS002523

Schulz, M., and Lanzerotti, L. J. (1974). Particle diffusion in the radiation belts. *Ser. Phys. Chem. Space* 7, 978-3-642-65677-4. doi:10.1007/978-3-642-65675-0

Spence, H. E., Reeves, G. D., Baker, D. N., Blake, J. B., Bolton, M., Bourdarie, S., et al. (2013). Science goals and overview of the radiation belt storm probes (RBSP) energetic particle, composition, and thermal plasma (ECT) suite on NASA's van allen probes mission. *Space Sci. Rev.* 179 (1–4), 311–336. doi:10.1007/s11214-013-0007-5

Sun, J., Gao, X., Lu, Q., Chen, L., Liu, X., Wang, X., et al. (2017). Spectral properties and associated plasma energization by magnetosonic waves in the Earth's magnetosphere: Particle-in-cell simulations. *J. Geophys. Res. Space Phys.* 122 (5), 5377–5390. doi:10.1002/2017ja024027

Teng, S., Li, W., Tao, X., Ma, Q., Wu, Y., Capannolo, L., et al. (2019). Generation and characteristics of unusual high frequency EMIC waves. *Geophys. Res. Lett.* 46 (14), 14230–14238. doi:10.1029/2019GL085220

Wu, Z., Su, Z., Liu, N., Gao, Z., Zheng, H., Wang, Y., et al. (2021). Off-equatorial source of magnetosonic waves extending above the lower hybrid resonance frequency in the inner magnetosphere. *Geophys. Res. Lett.* 48, e2020GL091830. doi:10.1029/2020GL091830

Wu, Z., Teng, S., Ma, Q., and Tao, X. (2022). A statistical study of pancake pitch angle distribution of low-energy protons and their correlation with magnetosonic waves. *JGR. Space Phys.* 127 (5), e2021JA030174. doi:10.1029/2021JA030174

Yuan, Z., Yu, X., Huang, S., Qiao, Z., Yao, F., and Funsten, H. O. (2018). Cold ion heating by magnetosonic waves in a density cavity of the plasmasphere. *J. Geophys. Res. Space Phys.* 123, 1242–1250. doi:10.1002/2017JA024919

Yue, C., Bortnik, J., Thorne, R. M., Ma, Q., An, X., Chappell, C. R., et al. (2017). The characteristic pitch angle distributions of 1 eV to 600 keV protons near the equator based on Van Allen Probes observations. *JGR. Space Phys.* 122, 9464–9473. doi:10.1002/2017JA024421